



Too many galaxy-galaxy strong lenses observed in galaxy clusters

M. Meneghetti^{1,2}, A. Ragagnin^{3,4,5}, S. Borgani^{6,4}, F. Calura¹, G. Despali⁷, C. Giocoli^{1,2,3}, G. L. Granato^{4,8,5}, C. Grillo^{9,10}, L. Moscardini^{3,1,2}, E. Rasia^{4,5}, et al.

The remaining authors can be found at the end of the paper.

¹ INAF-Osservatorio di Astrofisica e Scienza dello Spazio di Bologna, Via P. Gobetti 93/3, I-40129 Bologna, Italy,

² INFN-Bologna, Viale Berti Pichat 6/2, I-40127 Bologna, Italy

³ Dip. di Fisica e Astronomia "Augusto Righi", Alma Mater Studiorum Università di Bologna, via Gobetti 93/2, I-40129 Bologna, Italy

⁴ INAF - Osservatorio Astronomico di Trieste, via G.B. Tiepolo 11, I-34143 Trieste, Italy

⁵ IFPU - Institute for Fundamental Physics of the Universe, Via Beirut 2, I-34014 Trieste, Italy

The remaining affiliations can be found at the end of the paper. e-mail: massimo.meneghetti@inaf.it

Received: 23-12-2022; Accepted: 05-05-2023

Abstract. We recently reported an excess by a factor ~ 10 of galaxy-galaxy strong lenses (GGSL) in a sample of galaxy clusters compared to predictions from hydrodynamical simulations in a Λ CDM cosmology. We quantify the impact of numerical resolution and of the galaxy formation model adopted in the simulations on the predicted GGSL probability. We find that changing the mass resolution by factors of 10 and 25, while using the same galaxy formation model, does not affect the GGSL probability. On the contrary, adopting an AGN feedback scheme that is less efficient at suppressing gas cooling and star formation leads to an increase in the GGSL probability by a factor of between 3 and 6. However, we notice that such simulations form overly massive galaxies whose contribution to the lensing cross section would be significant but that their Einstein radii are too large to be consistent with the observations. Thus, although we find that the GGSL probability is sensitive to the galaxy formation model implemented in the simulations, all the tested models fail to explain the origin of the excess of GGSL we have reported.

Key words. cosmology: dark matter, galaxy clusters:gravitational lensing

1. Introduction

In the Λ CDM cosmological model, gravitationally bound dark-matter halos form hierarchically, with the most massive systems forming through mergers of smaller ones. As struc-

ture assembles in this fashion, large dark-matter halos contain smaller-scale substructure in the form of embedded subhalos. Such prediction can be verified in cosmic structures such as galaxy clusters, provided that one can recover their mass distribution.

In fact, being the most massive gravitationally bound structures in the universe, galaxy clusters are powerful gravitational lenses. When distant background galaxies are in near-perfect alignment with the massive foreground cluster, strong gravitational lensing occurs. Strong lensing, nonlinear effects produced by the deflection of light, results in multiple distorted images of individual background galaxies. By modeling a large set of strong lensing features, the inner structure of cluster dark matter halos can be recovered down to galaxy scale, provided that a sufficient number of multiple images with spectroscopic redshift information is available (Bergamini et al., 2019, 2021).

The strength of nonlinear strong lensing effects in the CDM paradigm can be predicted theoretically from simulations of structure formation. These simulations include complex galaxy formation models that describe phenomena such as gas cooling, star formation, and energy feedback from stars and Active-Galactic-Nuclei (AGNs). The lensing properties of the simulated galaxy clusters and of their galaxy members can be computed using ray-tracing techniques (e.g., Meneghetti et al., 2010, 2017).

In previous work, we tested the predictions of the Λ CDM cosmological model by comparing the ability of observed and simulated cluster galaxies to produce strong gravitational lensing events (Meneghetti et al., 2020, ME20 hereafter). We found that observed clusters produce an excess of galaxy-galaxy strong lensing (GGSL) events by a factor ~ 10 compared to CDM simulations. These results indicate that cluster galaxies are efficient strong lenses because they are unexpectedly compact. We conclude that an unidentified problem either with current simulation methods or incorrect assumptions about the properties of dark matter could explain our results. Understanding this issue and further stress-testing the CDM paradigm requires us to urgently investigate more lenses and, at the same time, carefully evaluate the limits of current simulations.

In this work, we study the impact of mass resolution and of several assumptions made in

the galaxy formation models on the theoretical estimates of GGSL probability from hydrodynamical simulations.

2. Observational dataset

We combine lensing data from the HST (from the CLASH and Frontier Fields surveys and from other GO programs) with spectroscopic data from the MUSE integral-field spectrograph at the Very Large Telescope to reconstruct the mass distribution of four galaxy clusters, namely Abell S1063 ($z = 0.3457$), MACS J0416.1-2403 ($z = 0.397$), MACS J1206.2-0847 ($z = 0.439$), and PSZ1 G311.65-18.48 ($z = 0.443$). Our methodology uses the so-called parametric approach implemented in the public code LENSTOOL (see, e.g., Kneib et al., 1996). It describes the cluster as a superposition of large-scale components to account for the large-scale cluster dark-matter halos, and small-scale components that describe the substructures. We associate the spatial positions of cluster member galaxies with the locations of dark-matter substructure. The mass distribution in these cluster galaxies is constrained using stellar kinematic measurements of cluster member galaxies from VLT spectroscopy. Each mass component is defined by a set of parameters, and, by searching the parameters that minimize the distance between the observed and model-predicted multiple images, we model the cluster mass distribution. The details of the mass reconstructions can be found in several previous papers (Bergamini et al., 2019, 2021; Pignataro et al., 2021).

3. Numerical simulations

The simulated cluster halos used in this work belong to a suite of numerical hydrodynamical simulations, dubbed the Dianoga suite. We focus on a sample of seven cluster-size halos, using the simulation outputs at six different redshifts between $z_{min} = 0.24$ and $z_{max} = 0.55$. The four clusters in the observational data set have redshifts in this range. Thus, we can compare them safely to the simulations. The clusters in the Dianoga sample were selected

in a dark matter-only large cosmological simulation and re-simulated at a higher resolution with the inclusion of baryons. We could compare several versions of these simulations spanning a range of galaxy formation models and spatial and force resolutions. In particular, in this work we compare:

- three versions of the Dianoga simulations implementing different schemes for AGN energy feedback, namely the models described by Rasia et al. (2015) (R15), Ragone-Figueroa et al. (2018) (RF18), and Bassini et al. (2020) (B20);
- for the B20 galaxy formation model, simulations employing three different levels of resolution. The lowest resolution simulations (dubbed 1x hereafter) correspond to masses of $8 \times 10^8 M_\odot$ and $1.5 \times 10^8 M_\odot$ per dark-matter and gas particles, respectively. In the higher resolution runs the particle masses are smaller by factors of 10x and 25x.

For each simulation snapshot, we generated three lens planes by projecting the particles within cylinders of depth 10 Mpc along the axes of the simulation box. We followed the procedure outlined in ME20 to produce the deflection angle, convergence and shear maps which cover a field-of-view of 200×200 arcsec and have 2048×2048 pixels.

4. GGSL probability

We compute the probability for galaxy-galaxy strong lensing for each simulated or observed cluster, as proposed by ME20. In short, the procedure involves the following steps: First, we use the lens model to compute the tangential critical lines for a given source redshift. We identify the critical lines connected to the cluster galaxies and exclude the critical lines corresponding to the large-scale cluster dark matter halo. We dub these critical lines secondary. We map them onto the source plane, obtaining the tangential caustics. In the case of the observed clusters, we perform this calculation using the deflection angle maps of the best-fit mass model.

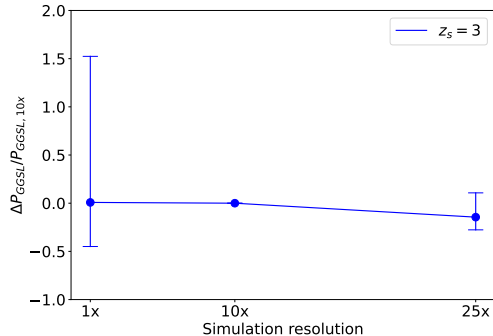


Fig. 1. Median relative change of GGSL probability with respect to the 10xB20 set, as a function of the mass resolution in the B20 simulations. The error bars show the 99% confidence limits.

For each caustic, we compute the enclosed area. Summing the areas $A_{cau,i}$ of all n_{cau} secondary caustics, we obtain the GGSL cross section, $\sigma_{GGSL}(z_S) = \sum_i^{n_{cau}} A_{cau,i}(z_S)$. Finally, we divide the GGSL cross section by the area sampled by the cluster mass reconstruction mapped onto the source plane, $A_{sp}(z_S)$, and we obtain the GGSL probability $P_{GGSL}(z_S) = \sigma_{GGSL}(z_S)/A_{sp}(z_S)$.

The same procedure is repeated for several source redshifts, namely $z_S = [1, 3, 6]$. We only consider the contribution to the GGSL probability from secondary critical lines with equivalent Einstein radii $\theta_E > 0.5$ arcsec. The choice is motivated by the resolution of the lensing maps (Meneghetti et al., 2022).

5. Results

We assess the impact of mass (and force) resolution on the GGSL probability by comparing the simulations' 1x, 10x, and 25x runs assuming the B20 galaxy formation model. In Fig. 1 we show the median relative variation of GGSL probability with respect to the 10xB20 set. The different simulation resolutions cause some variations in the cluster' evolutionary stage. Thus, the mass maps corresponding to the same cluster at a given redshift are not perfectly identical across the 1x, 10x, and 25x realizations. For this reason, the error bars are quite large. Nevertheless, on average, the GGSL probability is nearly independent of

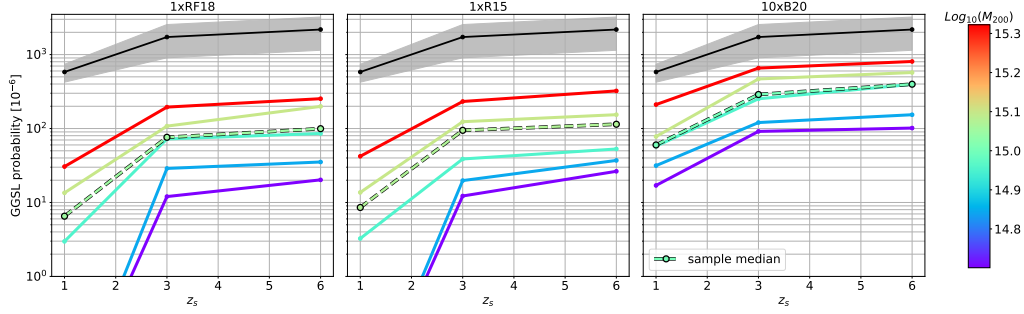


Fig. 2. GGSL probability as a function of the source redshift. The mean GGSL probability in the observational sample is shown with the solid black line in all panels. The gray color band shows the 99% confidence interval, computed by bootstrap sampling. The results for the 1xRF18, 1xR15, and 10xB20 simulation sets are shown in the left, central, and right panels, respectively. Each solid colored line corresponds to the median of GGSL probability in mass bins. The colors reflect the cluster mass, as indicated in the color bar on the right. The dashed black lines show the sample median probability, calculated using all cluster projections. Even with the B20 AGN feedback scheme, the GGSL probability of simulated clusters remains below the values measured in the observational dataset.

resolution. We show the results for a source redshift of $z_s = 3$. They are similar for other source redshifts.

On the contrary, the AGN scheme implemented in the simulations has a stronger impact on the GGSL probability. The RF18 and R15 models are characterized by feedback schemes that, despite their different implementation, have similarly high efficiency at suppressing star formation in massive cluster galaxies. Instead, the feedback scheme of B20 results in a higher star formation. Such higher star formation leads to the formation of overly massive cluster galaxies, where the condensation of stars in the center also drives the adiabatic contraction of the host dark matter halos. As a result, the cluster galaxies in the B20 simulations are stronger lenses, as shown in Fig. 2. For example, the GGSL probability in the 10xB20 set is higher by a factor of 3 to 6 than in the 1xRF18 or 1xR15 sets, depending on the cluster mass. Note, however, that even with the B20 AGN feedback scheme, the GGSL probability of simulated clusters remains below the values measured in the observational dataset (shown in gray).

The lower overall efficiency of the energy feedback leads to the formation of overly massive galaxies. For example, B20 show that the subhalo mass function in their simulations has

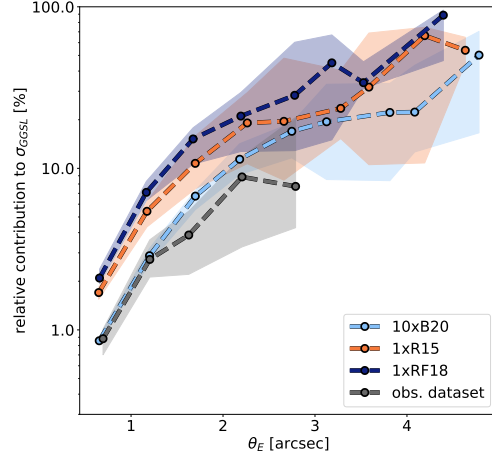


Fig. 3. Median relative contribution of galaxies with Einstein radius θ_E to the GGSL cross section of the host cluster. We assume $z_s = 6$. The dashed black line shows the results for the observational data set. The dashed light blue, orange, and dark blue lines refer to the 10xB20, 1xR15, and 1xRF18 simulation data sets, respectively. The colored bands show the 99% confidence limits of the median.

an excess in the high mass end. Moreover, their Brightest-Central-Galaxies are too large compared to observations. These massive galaxies have extended Einstein radii. They provide a

significant fraction of the GGSL cross-section. In Fig. 3, we show the relative contribution of galaxies with a given Einstein radius θ_E to the total GGSL cross-section of their host cluster. We quantify it by computing the median ratio between each galaxy cross-section (i.e., the area of its caustic) and the cluster GGSL cross-section in bins of equal Einstein radius. Using different colors, we show the results for the observational and the 10xB20, 1xR15, and 1xRF18 simulation data sets. The figure shows that individual galaxies in the observational data set typically contribute to only a few percent of the total GGSL cross-section of their host cluster. In other words, the total GGSL cross-section results from many contributing galaxies. On the contrary, fewer galaxies contribute to the GGSL cross-sections of simulated clusters. For example, the galaxies with Einstein radii $\theta_E > 3''$ contribute to 50-90% of the total GGSL cross-section. Given that these galaxies are missing in the observational data set, we do not count them when computing the GGSL probability shown in Fig. 2.

6. Conclusions

Based on the results discussed above, we reaffirm the tension between observations of GGSL and theoretical expectations in the framework of the Λ CDM cosmological model. We demonstrated that our conclusions do not depend on our simulations' mass and force resolution. We find that the GGSL probability is sensitive to the galaxy formation model implemented in the simulations. Still, all the tested models have difficulty simultaneously reproducing the stellar mass function and the internal structure of galaxies. For example, weaker AGN feedback would help make the galaxies more compact by enhancing star formation in the central regions. Such increased compactness would bring the GGSL probability closer to observations. However, such AGN feedback schemes produce overly massive galaxies with unrealistically large Einstein radii, which are not observed in our studied galaxy clusters.

Authors

G. Angora^{11,13}, L. Bassini¹², P. Bergamini^{9,1}, G. Granata⁹, A. Mercurio¹³, R. B. Metcalf^{3,1}, P. Natarajan¹⁴, M. Nonino⁴, G. Venusta Pignataro^{3,18}, C. Ragone-Figueroa^{8,15,4}, E. Vanzella¹, A. Acebron⁹, K. Dolag^{16,17}, G. Murante⁴, G. Taffoni⁴, L. Tornatore⁴, L. Tortorelli¹⁶, M. Valentini¹⁶, P. Rosati¹¹

Affiliations

⁶ZAH, Institut für Theoretische Astrophysik, Albert-Ueberle-Str. 2, D-69120 Heidelberg, Germany

⁷IATE, CONICET, Universidad Nacional de Córdoba, Laprida 854, X5000BGR, Córdoba, Argentina

⁸Dip. di Fisica, Università degli Studi di Milano, Via Celoria 16, I-20133 Milano, Italy

⁹INAF - IASF Milano, via A. Corti 12, I-20133 Milano, Italy

¹⁰Dip. di Fisica e Scienze della Terra, Università degli Studi di Ferrara, Via Saragat 1, I-44122 Ferrara, Italy

¹¹Center for Theoretical Astrophysics and Cosmology, Institute for Computational Science, University of Zurich, Winterthurerstrasse 190, CH-8057 Zürich, Switzerland

¹²INAF-Osservatorio Astronomico di Capodimonte, Via Moiariello 16, 80131 Napoli, Italy

¹³Department of Astronomy, Yale University, New Haven, CT, USA

¹⁴Observatorio Astronómico de Córdoba, Universidad Nacional de Córdoba, Laprida 854, X5000BGR, Córdoba, Argentina

¹⁵Universitäts-Sternwarte, Fakultät für Physik, Ludwig-Maximilians-Universität München, Scheinerstr.1, 81679 München, Germany

¹⁶Max-Planck-Institut für Astrophysik (MPA), Karl-Schwarzschild Strasse 1, D-85748 Garching bei München, Germany

¹⁷INAF - Istituto di Radioastronomia di Bologna, Via Gobetti 101, I-40129 Bologna, Italy

References

- Bassini, L., Rasia, E., Borgani, S., et al. 2020, *A&A*, 642, A37
- Bergamini, P., Rosati, P., Mercurio, A., et al. 2019, *A&A*, 631, A130
- Bergamini, P., Rosati, P., Vanzella, E., et al. 2021, *A&A*, 645, A140
- Kneib, J. P., Ellis, R. S., Smail, I., Couch, W. J., & Sharples, R. M. 1996, *ApJ*, 471, 643
- Meneghetti, M., Rasia, E., Merten, J., et al. 2010, *A&A*, 514, A93
- Meneghetti, M., Natarajan, P., Coe, D., et al. 2017, *MNRAS*, 472, 3177
- Meneghetti, M., Davoli, G., Bergamini, P., et al. 2020, *Science*, 369, 1347
- Meneghetti M., Ragagnin A., Borgani S., Calura F., Despali G., Giocoli C., Granato G. L., et al., 2022, arXiv, arXiv:2204.09065
- Pignataro, G. V., Bergamini, P., Meneghetti, M., et al. 2021, *A&A*, 655, A81
- Ragagnin, A., Meneghetti, M., Bassini, L., et al. 2022, *A&A*, 665, A16
- Ragone-Figueroa, C., Granato, G. L., Ferraro, M. E., et al. 2018, *MNRAS*, 479, 1125
- Rasia, E., Borgani, S., Murante, G., et al. 2015, *ApJ*, 813, L17